

# Strain enhanced superconductivity of $\text{MoX}_2$ ( $X=\text{S}$ or $\text{Se}$ ) bilayers with Na intercalation

Jun-Jie Zhang, Bin Gao, and Shuai Dong\*

Department of Physics, Southeast University, Nanjing 211189, China

(Dated: October 15, 2018)

$\text{MoX}_2$  ( $X=\text{S}$  or  $\text{Se}$ ) is a semiconductor family with two-dimensional structure. And a recent calculation predicted the superconductivity in electron doped  $\text{MoS}_2$  monolayer. In this work, the electronic structure and lattice dynamics of  $\text{MoX}_2$  bilayers with monolayer Na intercalated, have been calculated. According to the electron-phonon interaction, it is predicted that these bilayers can be transformed from indirect-gap semiconductors to a superconductors by Na intercalation. More interestingly, the biaxial tensile strain can significantly enhance the superconducting temperature up to  $\sim 10$  K in Na-intercalated  $\text{MoS}_2$ . In addition, the phonon mean free path at room-temperature is also greatly improved in Na intercalated  $\text{MoSe}_2$ , which is advantaged for related applications.

PACS numbers: 63.22.Np, 74.78.-w, 65.80.-g

## I. INTRODUCTION

Two-dimensional (2D) material such as graphene, black phosphorus, and layered transition metal dichalcogenides (TMDs) have attracted enormous interest for their unique structure, novel physical properties, and broad potential applications. Superior to the semi-metallic graphene, few-layer  $\text{MoS}_2$ 's show moderate band gaps which are crucial for practical on/off ratio in electronic circuit devices.<sup>1</sup> Besides,  $\text{MoS}_2$  is potentially important in optoelectronic because its band gap is in the visible light range.<sup>2</sup> For this reason, great efforts have been made to investigate the dynamics of various carriers in  $\text{MoS}_2$  including mobilities of electrons, excitons, as well as phonons.<sup>3-6</sup>

Structurally, each layer of  $\text{MoS}_2$  (as well as  $\text{MoSe}_2$ ) is constructed by the S-Mo-S (or Se-Mo-Se) sandwich, as shown in Fig. 1. Along the  $c$ -axis, the neighboring triatomic layer is weakly coupled by van der Waals (vdw) interaction.<sup>7</sup> This layered nature makes  $\text{MoS}_2$  (or  $\text{MoSe}_2$ ) flexible and tailorable, e.g. to be doped by ion absorption or intercalation, as well as to fabricate heterostructures.<sup>8-10</sup> These artificial modificatory  $\text{MoS}_2$  and  $\text{MoSe}_2$  show lots of extraordinary qualities. For example, a giant Rashba-type splitting was found in  $\text{MoS}_2/\text{Bi}(111)$  heterostructure,<sup>8</sup> and a half-metal behavior was predicted in Fe adatoms adsorbed on monolayer and bilayer  $\text{MoS}_2$  sheets.<sup>9</sup> Recently, the electron-doped monolayer  $\text{MoS}_2$  was predicted to be a BCS-type superconductor with a considerable critical temperature ( $T_C$ ) up to 20 K when one extra electron artificially-added per chemical unit.<sup>10</sup> However, by considering realistic doping methods (e.g. K absorption),<sup>10</sup> the calculated  $T_C$  was far below the expected value. Experimentally, an early work by Woollam *et al.* studied the insertion of K/Na atoms into bulk  $\text{MoS}_2$ , which found the maximum superconducting  $T_C$ 's of  $\text{K}_x\text{MoS}_2$  and  $\text{Na}_x\text{MoS}_2$  to be about 7 K and 3.2 K respectively.<sup>11</sup> In this sense, the electron doped  $\text{MoS}_2$  should be a promising superconductor although its real  $T_C$  is seriously suppressed by real doping methods. Very recently, the dynamical stability and su-

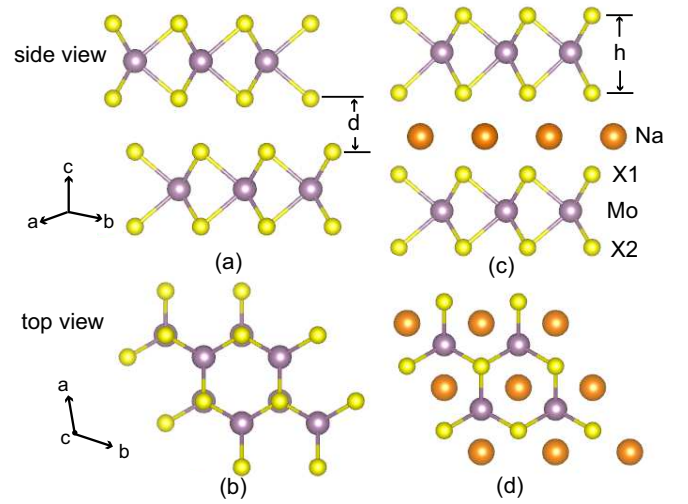


FIG. 1. (Color online) Side and top views of atomic structures of  $\text{MoX}_2$  bilayer [(a) and (b)] and  $(\text{MoX}_2)_2\text{Na}$  system [(c) and (d)].

perconductivity have been reported in the free-standing Li-intercalated  $\text{MoS}_2$ .<sup>12</sup> However, in real situation these 2D few layers are putted on particular substrates and will be affected by the lattice mismatch, which have not been addressed in Ref. 12.

In this work, the lattice dynamics and electron-phonon (EP) coupling of Na-intercalated  $\text{MoS}_2$  and  $\text{MoSe}_2$  bilayers have been studied via first-principles density functional theory (DFT) and density function perturbation theory (DFPT). Our calculations confirm the superconductivity in  $\text{MoS}_2$  and  $\text{MoSe}_2$  with Na intercalation. More interestingly, this superconductivity can be significantly enhanced by tensile strain. Our calculations will motivate more experimental studies to tune the physical properties like superconductivity of 2D materials by the strain effect.

## II. MODEL & METHODS

The DFT calculations have been performed using the PWSCF program of the Quantum-ESPRESSO distribution.<sup>13</sup> The ultrasoft pseudo-potential (including the semicore electrons as valence electrons in case of Mo) and generalized gradient approximation of Perdew-Burke-Ernzerhof (GGA-PBE) are used with a cutoff energy 35 Ry for the expansion of the electronic wave function in the plane waves. The vdw interactions are treated using the (Grimme) DFT-D2 approximation.<sup>14</sup>

MoX<sub>2</sub> bilayers are modeled using slabs with one Na layer (one Na per one unit cell area) inserted. The surfaces are simulated by adding a vacuum layer of  $\sim 15$  Å. For the electronic structure calculations, the Brillouin zone (BZ) integrations are performed with an  $18 \times 18 \times 1$  grid by using the first-order Hermite-Gaussian smearing technique. Within the framework of the linear response theory, the dynamical matrices are calculated for  $6 \times 6 \times 1$  grid of special  $q$  points in the irreducible two-dimensional BZ and are Fourier interpolated throughout the full Brillouin zone. The dense  $36 \times 36 \times 1$  grid is used in the BZ integrations in order to produce the accurate electron-phonon (EP) interaction matrices.

## III. RESULTS & DISCUSSION

### A. Crystalline & electronic structures

Although the stablest MoX<sub>2</sub> bilayers are stacked as the A-B type (Fig. 1(a-b)),<sup>15</sup> this type of stacking conformation becomes dynamic unstable when Na monolayer is interacted into the MoX<sub>2</sub> bilayers, as evidenced by the imaginary frequencies of phonon spectrum around  $\Gamma$  point. Alternatively, the A-A type stacking conformation (Fig. 1(c-d)) is dynamic stable, which will be further discussed in Sec.III.B. Similar conclusion was also recently reported in Li-interacted MoS<sub>2</sub> bilayer.<sup>12</sup> Therefore, considering the dynamic stabilization, the conformation as sketched in Fig. 1(d) will be systematically studied in the following. Each primitive cell contain two MoX<sub>2</sub> layers and one Na atom.

First, the relaxation is performed until the force on each atom is smaller than  $10^{-4}$  Ry/a.u.. The optimized lattice constant and interatomic distances are listed in Table I in comparison with the experimental values. The calculated lattice constant is only slight larger than the experimental value, which is quite reasonable since GGA normally overestimates lattice constants.

The calculated electron density difference are visualized in Fig. 2, which indicates the spatial distribution difference of electron density between the pure MoX<sub>2</sub> bilayer and Na-intercalated MoX<sub>2</sub> bilayer. The charge transfer from Na to X1 is obvious, especially for X=S, which changes the vdw force between original bilayers to ionic-bond-like interactions between Na and X1. As a direct result, the layer distance ( $d$ ) is significantly shorten,

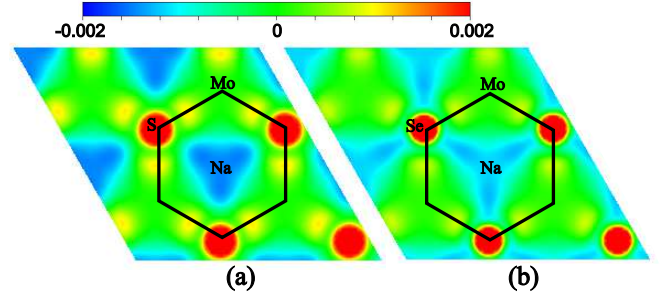


FIG. 2. (Color online) Electron density difference viewed along the (001) direction for (a) (MoS<sub>2</sub>)<sub>2</sub>Na and (b) (MoSe<sub>2</sub>)<sub>2</sub>Na.

TABLE I. The optimized structural parameters (as defined in Fig. 1) in unit of Å. The experimental values (with the superscript  $E$ ) are also listed.<sup>16,17</sup>

	MoS <sub>2</sub> <sup>E</sup>	MoS <sub>2</sub>	(MoS <sub>2</sub> ) <sub>2</sub> Na	MoSe <sub>2</sub> <sup>E</sup>	MoSe <sub>2</sub>	(MoSe <sub>2</sub> ) <sub>2</sub> Na
$a$	3.161	3.204	3.251	3.285	3.330	3.385
$h$	3.072	3.119	3.130	3.225	3.344	3.346
$d$	3.074	3.113	2.249	3.225	3.178	2.435

as listed in Table I.

The calculated band structures and density of states (DOS) are shown in Fig. 3. As expected, the Fermi level crosses the conduction band as a direct result of Na intercalation, which dopes electrons to X1's  $p$  orbitals and builds strong ionic bonding between Na-X. It should be noted that this intercalation is different from previously studied Na-adsorption on MoS<sub>2</sub> by Komesu *et.al.*,<sup>18</sup> who found a semiconductor behavior with a narrowed band gap.

### B. Phonon, electron-phonon coupling, & superconductivity

Then we turn to pay attention to the phonon modes at the zone center. The pure MoS<sub>2</sub> and MoSe<sub>2</sub> bilayers have the identical point group ( $D_{3d}$ ), which is reduced to  $D_{3h}$  in (MoX<sub>2</sub>)<sub>2</sub>Na. For the  $D_{3d}$  point group, the optical modes at BZ center  $\Gamma$  point can be decomposed as  $3A_{1g} \oplus 2A_{2u}$  polarized along the hexagonal  $c$  axis direction and  $3E_g \oplus 2E_u$  polarized in the hexagonal closed packed plane. The phonon modes  $E_g$  and  $A_{1g}$  are both Raman (R) active, while the  $A_{2u}$  and  $E_u$  modes are infrared (IR) active, as sketched in Fig. 4(a). In contrast, for the  $D_{3h}$  point group, the optical modes at  $\Gamma$  point can be decomposed as  $A_2'' \oplus A_1' \oplus E' \oplus E''$ .  $A_2''$  and  $E''$  are infrared active, while  $A_1'$  and  $E'$  are Raman active. The calculated frequencies of these optical modes are listed in Table II, in comparison with some experimental data.

For pure MoX<sub>2</sub> bilayers, the calculated phonon frequencies are only slightly smaller than the corresponding experimental values.<sup>19</sup> This tiny inaccuracy is un-

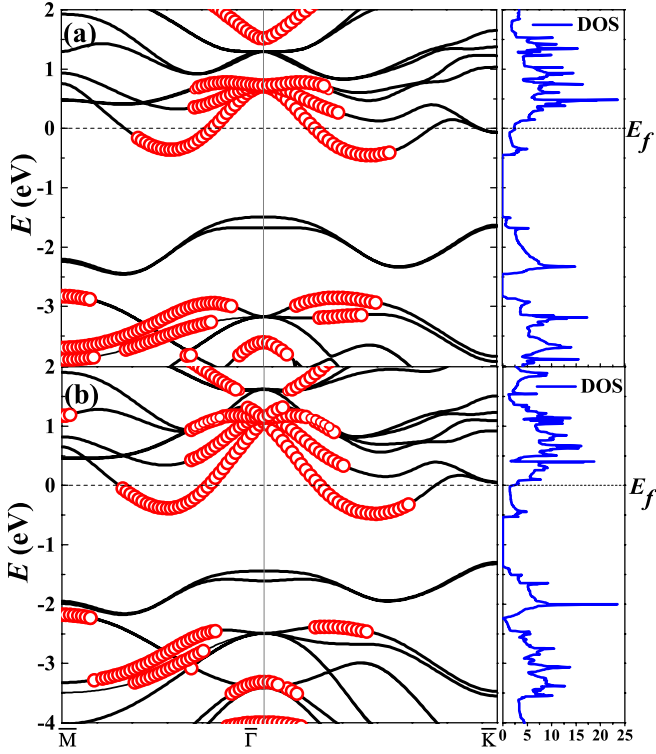


FIG. 3. (Color online) Electronic band structures and DOS's. The red circles indicate those states with more than 50% of density contributed by Na and X1. (a)  $(\text{MoS}_2)_2\text{Na}$ ; (b)  $(\text{MoSe}_2)_2\text{Na}_2$ .

TABLE II. The calculated frequencies (in unit of  $\text{cm}^{-1}$ ) of vibratory modes at  $\Gamma$  point for  $(\text{MoX}_2)_2\text{Na}$  system and pure  $\text{MoX}_2$  bilayer. The experimental values of  $A_{1g}^2$  ( $A_{2u}^2$ ) and  $E_g^1$  ( $E_u^1$ ) for pure  $\text{MoS}_2$  ( $\text{MoSe}_2$ ) bilayer are  $406.1 \text{ cm}^{-1}$  ( $242.8 \text{ cm}^{-1}$ ) and  $384.9 \text{ cm}^{-1}$  ( $287.1 \text{ cm}^{-1}$ ), respectively.<sup>19</sup>

R	$A_{1g}^1$	$A_{2g}^2$	$E_g^1$	$E_g^2$	$A_{1g}^3$	$E_g^3$
$\text{MoS}_2$	464.3	398.9	376.7	280.9	25.6	20.3
$\text{MoSe}_2$	345.1	237.6	277.6	163.7	36.2	18.7
R	$A_1'(1)$	$A_1'(2)$	$E'(1)$	$E'(2)$	$A_1'(3)$	$E'(3)$
$(\text{MoS}_2)_2\text{Na}$	416.9	329.0	349.3	260.6	39.0	15.9
$(\text{MoSe}_2)_2\text{Na}$	313.2	206.3	260.4	154.8	29.5	19.2
IR	$A_{2u}^1$	$A_{2u}^2$	$E_u^1$	$E_u^2$		
$\text{MoS}_2$	462.6	405.4	376.7	280.2		
$\text{MoSe}_2$	344.1	235.7	277.1	163.1		
IR	$A_2''(1)$	$A_2''(2)$	$E''(1)$	$E''(2)$		
$(\text{MoS}_2)_2\text{Na}$	416.5	321.3	349.3	257.1		
$(\text{MoSe}_2)_2\text{Na}$	311.7	205.2	260.6	156.0		

derstandable since the GGA-PBE pseudo-potential normally overestimates the volume of cell, which softens the phonon modes. For  $(\text{MoX}_2)_2\text{Na}$  systems, there are considerable red shifts of phonon frequencies compared to the corresponding ones of pure  $\text{MoX}_2$  bilayers except  $A_1'(3)$  for  $(\text{MoS}_2)_2\text{Na}$  and  $E'(3)$  for  $(\text{MoSe}_2)_2\text{Na}$ . On

one hand, the expanded lattice structure by the intercalated Na layer (e.g. see  $a$ 's and  $h$ 's in Table I) leads to weaker force constants between X-Mo, which softens phonon modes. In fact, due to a larger lattice constant of  $(\text{MoSe}_2)_2\text{Na}$  compared with  $(\text{MoS}_2)_2\text{Na}$ , the frequencies of phonon modes in  $(\text{MoSe}_2)_2\text{Na}$  are correspondingly smaller than those of  $(\text{MoS}_2)_2\text{Na}$ . On the other hand, the aforementioned charge transfer from Na to X1 makes the X1-Na links be strongly ionic-type, which may suppress the neighbor covalent X-Mo bonds as a side effect. The  $A'(3)$  and  $E'(3)$  mode, which are layer and shear breathing modes respectively, are sensitive to the interlayer interaction. Due to the electronegativity difference between S and Se, more (less) charge is transferred from Na to neighboring S (Se), making stronger (weaker) Coulomb attraction between Na monolayer and  $\text{MoS}_2$  ( $\text{MoSe}_2$ ) layers. Thus, the changes of  $A'(3)$  and  $E'(3)$  modes in  $\text{Na}(\text{MoSe}_2)_2$  are analogous to the trilaminar  $\text{MoSe}_2$  case,<sup>19</sup> i.e.  $A'(3)$  is softening and  $E'(3)$  is stiffening. In contrast, the strong Coulomb attraction between Na monolayer and  $\text{MoS}_2$  layer moves these two modes toward opposite directions, i.e.  $A'(3)$  is blue shifted and  $E'(3)$  is red shifted, similar to the Li-intercalated  $\text{MoS}_2$  case.<sup>12</sup>

The calculated phonon dispersions along major high symmetry lines and phonon densities of states (PDOS,  $F(\omega)$ ) for  $(\text{MoX}_2)_2\text{Na}$  are shown in Fig. 4(b-e). No imaginary frequency exists in the full phonon spectra, indicating the dynamical stability of the calculated structures of  $(\text{MoX}_2)_2\text{Na}$ . Since Na's vibration modes own the identical symmetry to these X-Mo-X ones, the phonon eigenvectors have a strongly mixed character of Na atom and  $\text{MoX}_2$  triatomic layer, as indicated in Fig. 4(b-c). It is clear that the vibrations contributed by Na are in the intermediate- and low-frequency region, as well as the out-of-plane acoustic mode (ZA). Generally, the acoustic modes and the layer-breathing modes for opposite vibrations of two triatomic layers are in the low-frequency range and the sandwich X-Mo-X bond-stretching modes are in the high-frequency range due to the strong covalent bonding.<sup>20</sup> As shown in Fig. 4(b), two interlayer-shear modes [ $E'(\text{TO})$ : optical in-plane transverse mode,  $E'(\text{LO})$ : optical in-plane longitudinal mode] and one interlayer-breathing mode [ $A_2''(\text{ZO})$ : optical out-plane mode] are highly mixed with the Na layer's contribution, especially for the  $E'(\text{LO})$  mode. And due to the moderate Coulomb attraction between Na and neighboring X1 ions, these  $E'(\text{TO})$ ,  $E'(\text{LO})$ , and  $A_2''(\text{ZO})$  modes situate in the intermediate frequency region.

In the following, the EP interaction is estimated. According to the Migdal-Eliashberg theory, the Eliashberg spectral function [ $\alpha^2 F(\omega)$ ] is given by:<sup>21</sup>

$$\alpha^2 F(\omega) = \frac{1}{N(E_f)} \sum_{\nu} \sum_{kqjj'} \left| g_{(k+q)j'kj}^{q\nu} \right|^2 \delta(\varepsilon_{kj} - \varepsilon_F) \delta(\varepsilon_{(k+q)j} - \varepsilon_F) \delta(\omega - \omega_{q\mu}) \quad (1)$$

where  $N(E_f)$  is the electronic DOS at Fermi level;

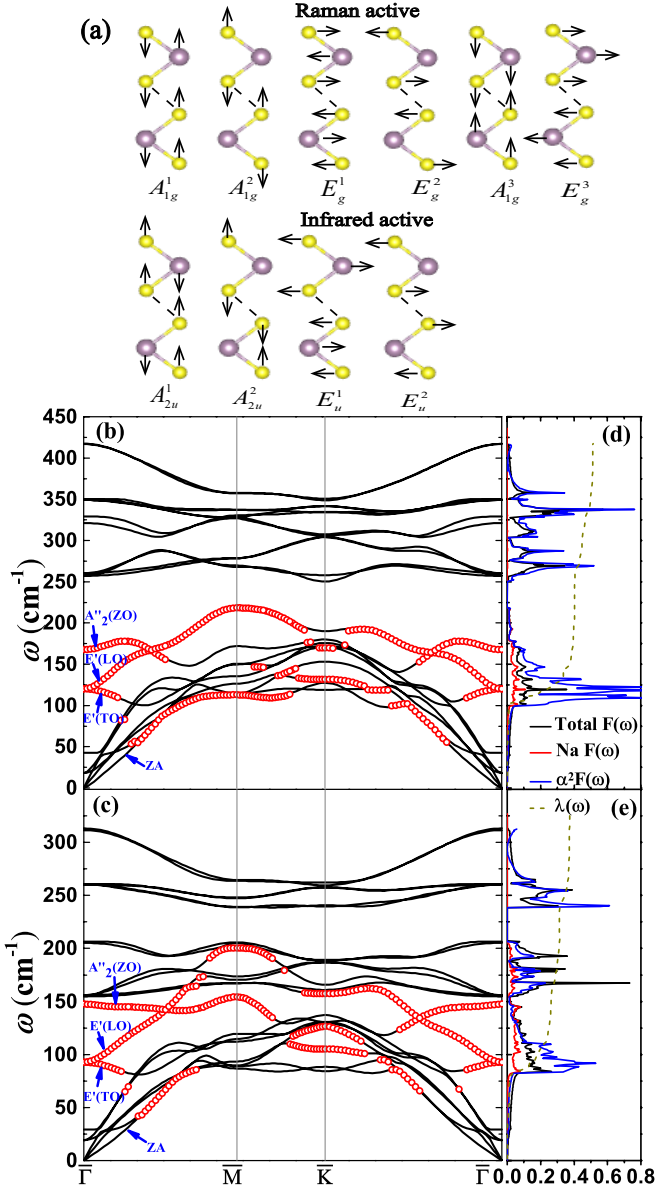


FIG. 4. (Color online) (a) Sketch of vibration modes of MoX<sub>2</sub> bilayer. (b-c) Calculated phonon dispersion, phonon DOS, electron-phonon coupling  $\lambda$ , and Eliashberg spectral function for (MoS<sub>2</sub>)<sub>2</sub>Na system [(b) and (d)] and for (MoSe<sub>2</sub>)<sub>2</sub>Na system [(c) and (e)].

$g_{(k+q)j'k_j}^{qv}$  is the EP matrix element which can be determined self-consistently by the linear response theory. The EP coupling coefficient  $\lambda$  is obtained by evaluating:<sup>22</sup>

$$\lambda = 2 \int_0^\infty \frac{\alpha^2 F(\omega)}{\omega} d\omega. \quad (2)$$

The calculated coefficients are summarized in Table III and the Eliashberg functions for (MoX<sub>2</sub>)<sub>2</sub>Na are shown in Fig. 4(c-d). The similarity between  $F(\omega)$  and  $\alpha^2 F(\omega)$  indicates that all vibration modes contribute to the EP interaction. However, those high-frequency phonons do not contribute much to the strength of electron-phonon

TABLE III. Calculated superconducting  $T_C$  in unit of K, electron-phonon coupling  $\lambda$ , logarithmically averaged frequency  $\omega_{ln}$  (in unit of K) and electronic DOS at Fermi level  $N(E_f)$  (states/eV).

	$N(E_f)$	$\omega_{ln}$	$\lambda$	$T_C$
(MoS <sub>2</sub> ) <sub>2</sub> Na	2.377	219.452	0.509	2.858
(MoSe <sub>2</sub> ) <sub>2</sub> Na	2.143	177.137	0.373	0.484

interaction due to the weighting of  $1/\omega$  in the definition of  $\lambda$  (see Eq. 2).

According to Fig. 4(d-e), it's obvious that  $E'(TO)$ ,  $E'(LO)$ , and  $A_2''(ZO)$  modes in (MoX<sub>2</sub>)<sub>2</sub>Na make great contribution to  $\lambda$  by increasing  $\alpha^2 F(\omega)$  curve peak in the low frequency region. As summarized in Table III,  $\lambda$  is larger in (MoS<sub>2</sub>)<sub>2</sub>Na than in (MoSe<sub>2</sub>)<sub>2</sub>Na. The physical reasons are: 1) Larger DOS value at the Fermi level in (MoS<sub>2</sub>)<sub>2</sub>Na; 2) The contribution from  $E'(TO)$ ,  $E'(LO)$ , and  $A_2''(ZO)$  modes are stronger in (MoS<sub>2</sub>)<sub>2</sub>Na.

The superconducting  $T_C$  can be estimated using the Allen-Dynes modified McMillan equation:<sup>23</sup>

$$T_C = \frac{\omega_{ln}}{1.2} \exp\left[-\frac{1.04(1 + \lambda)}{\lambda - \mu^*(1 + 0.62\lambda)}\right], \quad (3)$$

where  $\mu^*$  is the Coulomb repulsion parameter and  $\omega_{ln}$  is the logarithmically averaged frequency. When taking a typical value  $\mu^* = 0.1$ , the calculated  $T_C$  is 2.858 K for (MoS<sub>2</sub>)<sub>2</sub>Na, which is very close to the measured values (about 2.2-3.2 K) for Na-doped MoS<sub>2</sub> bulk.<sup>11</sup> However, the obtained  $T_C$  (0.484 K) for (MoSe<sub>2</sub>)<sub>2</sub>Na is very low.

The substrate strain from lattice mismatch is a widely used method to tune the physical properties of 2D materials, e.g. zero-field quantum Hall effect in graphene.<sup>24</sup> Then it is interesting to study the lattice mismatch effect to the superconducting  $T_C$  of Na-intercalated MoX<sub>2</sub>.

The biaxial strain ( $\epsilon$ ) is imposed to simulate the lattice mismatch and the results are shown in Fig. 5. Interestingly, for (MoS<sub>2</sub>)<sub>2</sub>Na with increasing tensile strain,  $T_C$  continuously increases to a maximum value 10.049 K at  $\epsilon = +7\%$ , beyond which  $T_C$  turns to decrease. In contrast, the compressive strain can suppress  $T_C$  monotonously, e.g. to 0.295 K when biaxial strain down to  $\epsilon = -5\%$ .

Physically, a tensile strain suppresses the bilayer thickness and thus shortens the distance between Na and S1, which can result in more electron transfer from Na to S1 and improve the DOS at the Fermi level (as shown in Fig. 5(b)). In addition, tensile strain also leads to stronger electron-phonon interaction by softening the  $E'(TO)$ ,  $E'(LO)$ , and  $A_2''(ZO)$  modes. Similar conclusion is also reached in (MoSe<sub>2</sub>)<sub>2</sub>Na whose  $T_C$  is enhanced up to 3.944 K for  $\epsilon = +5\%$  biaxial tensile strain but suppressed to near zero for compressive strain.

Previous studies suggested that in general the superconducting  $T_C$  of 2D materials could be improved by increasing doping density.<sup>10,20,25</sup> Our calculation gives one more route to improve  $T_C$  effectively and easily.



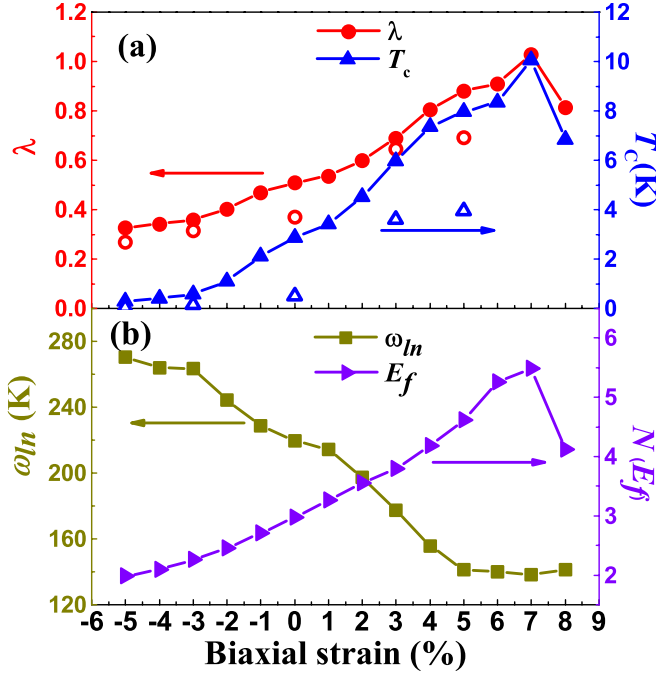


FIG. 5. (Color online) Calculated biaxial stress effects for (MoX<sub>2</sub>)<sub>2</sub>Na (solid symbols: (MoS<sub>2</sub>)<sub>2</sub>Na; open symbols: (MoSe<sub>2</sub>)<sub>2</sub>Na). The dynamic stability for both cases persists within this strain region. (a) Superconducting T<sub>C</sub> (right axis) and electron-phonon coupling λ (left axis). (b) Logarithmically averaged frequency ω<sub>ln</sub> and electronic DOS at Fermi level N(E<sub>f</sub>).

### C. Phonon mean free path

Finally, in order to deeply understand the lattice dynamics of Na-intercalated MoX<sub>2</sub>, the phonon mean free path (MFP) is also investigated, which now can be directly measured in experiments.<sup>26</sup> The phonon MFP for the mode at  $q$  point with  $s$  polarization is defined as  $Q_{qs} = V_{qs}\tau_{qs}$ , where  $V_{qs}$  is the phonon group velocity and  $\tau_{qs}$  is phonon relaxation time. In real materials, the phonon relaxation time is determined by the combination of electron-phonon, phonon-phonon umklapp scattering, and boundary scattering. For few-layer 2D materials, the boundary scattering from the sides should be very weak and negligible.<sup>27</sup> For simplify, a uniform lifetime ( $\tau^{ep}$ ) is assumed for all phonon modes' contributions to the electron-phonon scattering, and the Debye spectrum is adopted as the phonon density of state approximatively<sup>28</sup>. Then,  $\alpha^2F(\omega)$  can be approximated as:<sup>28</sup>

$$\alpha^2F(\omega) \approx \frac{3(\tau^{ep})^{-1}}{2\pi N(E_f)} \frac{\omega}{\hbar\omega_D^3}, \quad (4)$$

where  $\omega_D$  is the Debye frequency. Corresponding the  $\lambda$  can be integrated as:

$$\lambda = 2 \int_0^\infty \frac{\alpha^2F(\omega)}{\omega} d\omega = \frac{6(\tau^{ep})^{-1}}{2\pi N(E_f)} \frac{1}{\hbar\omega_D^2}. \quad (5)$$

TABLE IV. The calculated Debye frequency  $\omega_D$ , phonon-phonon relaxation time ( $\tau^{ph-ph}$ ), electron-phonon relaxation time ( $\tau^{ep}$ ), and MPF for (MoX<sub>2</sub>)<sub>2</sub>Na system around the  $\Gamma$  point at room temperature and at the frequency of 4 cm<sup>-1</sup>.

	$\omega_D$ (cm <sup>-1</sup> )	$\tau^{ph-ph}$ (ps)	$\tau^{ep}$ (ps)	MPF (nm)
(MoS <sub>2</sub> ) <sub>2</sub> Na	237.0	237.4 (TA)	23.8	142.4 (TA)
		236.8 (LA)		229.9 (LA)
(MoSe <sub>2</sub> ) <sub>2</sub> Na	171.9	1077.2 (TA)	68.5	536.2 (TA)
		913.6 (LA)		612.3 (LA)

Then using the value of  $\lambda$  calculated before, the effective  $\tau^{ep}$  can be estimated, as presented in Table IV.

The three-phonon umklapp scattering lifetimes ( $\tau^{ph-ph}$ ) for different phonon branches can be estimated as:<sup>29,30</sup>

$$\tau_{qs}^{ph-ph} = (2\gamma_{qs}^2 \frac{k_B T}{M v_s^2} \frac{\omega_{qs}^2}{\omega_D})^{-1}, \quad (6)$$

where  $M$  is the mass of a (MoX<sub>2</sub>)<sub>2</sub>Na unit cell,  $v_s$  is the average phonon velocity for a given branch,  $T$  is temperature,  $k_B$  is the Boltzmann constant, and  $\gamma$  is the Grüneisen parameter. For 2D materials, the  $\gamma$  of each phonon mode at  $q$  point with  $s$  polarization is given by:<sup>31,32</sup>

$$\gamma_{qs} = -\frac{a}{2\omega_s(q)} \frac{d\omega_s(q)}{da} \quad (7)$$

Since the acoustic modes (particularly the LA and TA modes) have relatively larger velocities around the  $\Gamma$  point than those of the optical modes, they contribute to most of  $Q$ .<sup>33</sup> Here  $\gamma_{qs}$  is averaged around  $\Gamma$  point. The calculated MFP's of acoustic modes around the  $\Gamma$  point are listed in Table IV. The phonon-phonon umklapp scattering makes about 90% contributions to MFP for (MoX<sub>2</sub>)<sub>2</sub>Na. The anharmonic terms in lattice vibration have great influences on MFP and mainly reflect in  $\gamma$  here. Generally, larger  $\gamma$  leads to smaller MFP. For (MoS<sub>2</sub>)<sub>2</sub>Na, we obtain  $\gamma$  for TA and LA modes are 2.64 and 2.11 respectively, while in (MoSe<sub>2</sub>)<sub>2</sub>Na are only 1.47 and 1.34 respectively. The stronger anharmonicity in (MoS<sub>2</sub>)<sub>2</sub>Na leads to smaller MFP. Therefore, the MFP's (536.2 nm for the TA branch, 612.3 nm for the LA branch) in (MoSe<sub>2</sub>)<sub>2</sub>Na is quite prominent, approaching that of graphene (about 775 nm).<sup>34</sup> Even for (MoS<sub>2</sub>)<sub>2</sub>Na, the MFP's (142.4 nm for the TA branch and 229.9 nm for the LA branch) are larger than those of monolayer MoS<sub>2</sub> (about 103.1 nm for the LA branch calculated using the same method). While in Ref. 35, the MFP for the LA branch was reported to be only 18.1 nm for MoS<sub>2</sub> monolayer, which was partially due to the inaccuracy  $\gamma$  in their calculation, as pointed out by Ref. 36 and 37. In short, the Na-intercalation can significantly improve the phonon mean free path of (MoX<sub>2</sub>)<sub>2</sub>Na, which may be used in heatconduction devices.

#### IV. CONCLUSION

An in-depth understanding of electronic properties, the lattice dynamical properties, and superconductivity of modificatory 2D materials is highly important for its potential applications in heatconduction devices as well as nanoscale superconductor. The present DFT study found that the Na atoms intercalation can effectively change the electronic properties and lattice dynamical properties of MoS<sub>2</sub> and MoSe<sub>2</sub>.

In summary, electrons transfer from intercalated Na atoms to neighboring Se or S atoms, which increase the

density of states at the Fermi level and a semiconducting-to-metallic transition. The superconductivity is expected to be induced by such Na-intercalation, and the superconducting  $T_C$  would be enhanced by biaxial tensile strain. In addition, the phonon mean free path at room-temperature is also greatly improved in Na intercalated MoSe<sub>2</sub>, which is advantaged for related applications.

#### ACKNOWLEDGMENTS

Work was supported by National Natural Science Foundation of China (Grant Nos. 11274060 and 51322206).

- 
- \* Corresponding author: sdong@seu.edu.cn
- <sup>1</sup> B. Radisavljevic, A. Radenovic, J. Brivio, V. Giacometti, and A. Kis, *Nature Nanotech.* **6**, 147 (2011).
  - <sup>2</sup> Q. H. Wang, K. Kalantar-Zadeh, A. Kis, J. N. Coleman, and M. S. Strano, *Nature Nanotech.* **7**, 699 (2012).
  - <sup>3</sup> S. Sim, J. Park, J. G. Song, C. In, Y. S. Lee, H. Kim, and H. Choi, *Phys. Rev. B* **88**, 075434 (2013).
  - <sup>4</sup> H. Shi, R. Yan, S. Bertolazzi, J. Brivio, B. Gao, A. Kis, D. Jena, G. H. Xing, and L. Huang, *ACS Nano* **7**, 1072 (2013).
  - <sup>5</sup> K. Kaasbjerg, K. S. Thygesen, and K. W. Jacobsen, *Phys. Rev. B* **85**, 115317 (2012).
  - <sup>6</sup> K. Kaasbjerg, K. S. Thygesen, and A. P. Jauho, *Phys. Rev. B* **87**, 235312 (2013).
  - <sup>7</sup> J. L. Verble and T. J. Wieting, *Phys. Rev. Lett.* **25**, 362 (1970).
  - <sup>8</sup> K. Lee, W. S. Yun, and J. D. Lee, *Phys. Rev. B* **91**, 125420 (2015).
  - <sup>9</sup> Z. Y. Huang, G. L. Hao, C. Y. He, H. Yang, L. Xue, X. Qi, X. Y. Peng, and J. X. Zhong, *J. Appl. Phys.* **114**, 083706 (2013).
  - <sup>10</sup> Y. Z. Ge and A. Y. Liu, *Phys. Rev. B* **87**, 241408 (2013).
  - <sup>11</sup> J. A. Woollam and R. B. Somoano, *Phys. Rev. B* **13**, 3843 (1976).
  - <sup>12</sup> G. Q. Huang, Z. W. Xing, and D. Y. Xing, *Phys. Rev. B* **93**, 104511 (2016).
  - <sup>13</sup> P. Giannozzi, S. Baroni, N. Bonini, M. Calandra, R. Car, C. Cavazzoni, D. Ceresoli, G. L. Chiarotti, M. Cococcioni, and I. D. et al., *J. Phys.: Condens. Matter* **21**, 395502 (2009).
  - <sup>14</sup> S. Grimme, *J. Comput. Chem.* **27**, 1787 (2006).
  - <sup>15</sup> Q. H. Liu, L. Li, Y. F. Li, Z. X. Gao, Z. F. Chen, and J. Lu, *J. Phys. Chem. C* **116**, 21556 (2012).
  - <sup>16</sup> T. Böker, R. Severin, A. Müller, C. Janowitz, R. Manzke, D. Voss, P. Krüger, A. Mazur, and J. Pollmann, *Phys. Rev. B* **64**, 235305 (2001).
  - <sup>17</sup> L. M. Kulikov, A. A. S. Kobzar, L. G. Akselrud, T. A. Lobova, and E. A. Bogachev, *Inorg. Mater.* **28**, 397 (1992).
  - <sup>18</sup> T. Komesu, D. Le, X. Zhang, Q. Ma, E. F. Schwier, Y. Kojima, M. Zheng, H. Iwasawa, K. Shimada, M. Taniguchi, L. Bartels, T. S. Rahman, and P. A. Dowben, *Appl. Phys. Lett.* **105**, 241602 (2014).
  - <sup>19</sup> S.-Y. Chen, C. Zheng, M. S. Fuhrer, and J. Yan, *Nano Lett.* **15**, 2526 (2015).
  - <sup>20</sup> G. Q. Huang, Z. W. Xing, and D. Y. Xing, *Appl. Phys. Lett.* **106**, 113107 (2015).
  - <sup>21</sup> G. Grimvall, *The electron-phonon interaction in metals*, Vol. 8 (North-Holland Amsterdam, 1981).
  - <sup>22</sup> P. B. Allen and M. L. Cohen, *Phys. Rev.* **187**, 525 (1969).
  - <sup>23</sup> P. B. Allen and R. C. Dynes, *Phys. Rev. B* **12**, 905 (1975).
  - <sup>24</sup> F. Guinea, M. Katsnelson, and A. Geim, *Nature Phys.* **6**, 30 (2010).
  - <sup>25</sup> M. Q. Xue, G. F. Chen, H. X. Yang, Y. H. Zhu, D. M. Wang, J. B. He, and T. B. Cao, *J. Am. Chem. Soc.* **134**, 6536 (2012).
  - <sup>26</sup> A. J. Minnich, J. A. Johnson, A. J. Schmidt, K. Esfarjani, M. S. Dresselhaus, K. A. Nelson, and G. Chen, *Phys. Rev. Lett.* **107**, 095901 (2011).
  - <sup>27</sup> Z. Wang and N. Mingo, *Appl. Phys. Lett.* **99**, 101903 (2011).
  - <sup>28</sup> P. Souvatzis, *J. Phys.: Condens. Matter* **23**, 445401 (2011).
  - <sup>29</sup> P. G. Klemens, *Journal of Wide Bandgap Materials* **7**, 332 (2000).
  - <sup>30</sup> P. G. Klemens, *Int. J. Thermophys.* **22**, 265 (2001).
  - <sup>31</sup> J. Zou and A. Balandin, *J. Appl. Phys.* **89**, 2932 (2001).
  - <sup>32</sup> N. Mounet and N. Marzari, *Phys. Rev. B* **71**, 205214 (2005).
  - <sup>33</sup> Z. Y. Ong and E. Pop, *Phys. Rev. B* **84**, 075471 (2011).
  - <sup>34</sup> S. Ghosh, I. Calizo, D. Teweldebrhan, E. P. Pokatilov, D. L. Nika, A. A. Balandin, F. M. W. Bao, and C. N. Lau, *Appl. Phys. Lett.* **92**, 151911 (2008).
  - <sup>35</sup> Y. Q. Cai, J. H. Lan, G. Zhang, and Y. W. Zhang, *Phys. Rev. B* **89**, 035438 (2014).
  - <sup>36</sup> L. F. Huang, P. L. Gong, and Z. Zeng, *Phys. Rev. B* **90**, 045409 (2014).
  - <sup>37</sup> C. Sevik, *Phys. Rev. B* **89**, 035422 (2014).